Selfie Drones for 3D Modelling, Geological Mapping and Data Collection: Key Examples from Santorini Volcanic Complex, Greece

Fabio Luca Bonali[1,2] [a], Varvara Antoniou[3] [b], Othonas Vlasopoulos[3] [c], Alessandro Tibaldi[1,2] [d]
and Paraskevi Nomikou[3] [e]

[1]*Department of Earth and Environmental Sciences, University of Milano-Bicocca,*
Piazza della Scienza 4 – Ed. U04, 20126, Milan, Italy
[2]*CRUST- Interuniversity Center for 3D Seismotectonics with Territorial Applications, Italy*
[3]*Department of Geology and Geoenvironment, National and Kapodistrian University of Athens,*
Panepistimioupoli Zografou, 15784 Athens, Greece
{fabio.bonali, alessandro.tibaldi}@unimib.it, {vantoniou, evinom}@geol.uoa.gr, othonvl@gmail.com

Abstract: In the present work, we tested the use of selfie drones as a tool for 3D modeling, geological mapping, and data collection. The model we used is a 0.300-kg multirotor quadcopter being equipped with a 1/2.3-inch CMOS sensor capable of capturing 12 Megapixel pictures, attached to a 2-axis mechanical gimble and with approximately 16 minutes of flight time. Test sites are located in Santorini and are characterised by different settings: i) the 1570-1573 AD volcanic crater area, in Nea Kameni island, has a mostly horizontal topography; ii) the outcrop along Vlychada beach, showing layers of the Late Bronze Age (also well-known as Minoan) eruption, has mostly vertical topography. By applying the Structure from Motion techniques to pictures collected using the selfie drone, we were capable of: i) reconstructing the two sites with centimetric to sub-centimetric resolution; ii) recognizing geological features on very high-resolution Digital Surface Models and Ortomosaics; iii) mapping vertical cliffs made up of volcanic deposits on 3D Digital Outcrops Models; iv) collect new quantitative data for both sites.

1 INTRODUCTION

Field studies and data collection are vital for mapping and understanding the active geological processes on Earth, particularly for those that induced superficial deformations like earthquakes and shallow magmatic processes (e.g. Bonali et al., 2012; Tibaldi et al., 2017). However, field studies and direct observations are very often limited by specific field-related conditions such as the inaccessibility of key outcrops due to their location in remote or dangerous areas (e.g. Tibaldi et al., 2008). The Structure from Motion and Multiview stereo (SfM-MVS) photogrammetry techniques, where photos are collected using Unmanned Aerial Vehicles (UAVs), are nowadays widely used in Earth and Environmental Sciences to overcome these problems providing high-resolution 3D Digital Outcrop Models (DOMs), digital surface models (DSMs) and Orthomosaics as results (e.g. Bonali et al., 2019a; Fallati et al., 2019). Most people dealing with geological and geohazard studies use different types of UAVs: balloons, multi-rotor, fixed-wing and hybrid. Whereas balloons do not need fuel or battery, on the other hand they cannot be remotely controlled. Hybrid types allow to switch between flying like a fixed-wing aircraft and hovering like a multi-rotor one. The fixed-wing type can cover larger areas in a smaller time frame using high quality cameras, but such model is more difficult to be transported and more expensive than multi-rotor UAVs. Based on our experience, the latter can fly at very low heights attaining a great field resolution, and

---

[a] https://orcid.org/0000-0003-3256-0793
[b] https://orcid.org/0000-0002-5099-0351
[c] https://orcid.org/0000-0002-6713-9141
[d] https://orcid.org/0000-0003-2871-8009
[e] https://orcid.org/0000-0001-8842-9730

much more importantly, take-off and landing operations are easier than for fixed-wing models; this is crucial especially in difficult logistic terrains (e.g. outcropping lavas, Bonali et al., 2019a).

In the present work we tested the use of the so called "selfie drones" - quadcopter type - to produce very high-detailed 3D DOMs of relevant outcrops for geological mapping, data collection and scientific dissemination. As case studies we selected two sites within the Santorini volcanic complex (Fig. 1) with different characteristics: *i*) the 1570-1573 AD volcanic crater in Nea Kameni island and *ii*) an outstanding vertical outcrop showing volcanic layered deposits, along the Vlychada Beach, southern Santorini (Fig. 1B).

2 GEOLOGICAL SETTING OF KEY SITES

Santorini volcanic group is a ring of three islands (Thera, Therasia, and Aspronisi) around a flooded caldera containing the islands of Palea and Nea Kameni, which postdate caldera collapse (3.6ka) and are the subaerial expressions of an intracaldera, largely submarine lava shield (Druitt, 2014). The caldera is a 11x7km composite structure resulting from at least four collapses over the last 200ky (Druitt and Francaviglia, 1992), the last of which took place during, and immediately following, the ~1630 BCE 'Minoan' eruption (Friedrich et al., 2006). It consists of three flat-floored basins: a large northern 390m deep, and two smaller ones (western: 320m and southern: 270m respectively, Nomikou et al., 2013).

The Kameni islands are the subaerial expression of a $4.3 \pm 0.7 \text{km}^3$ intracaldera shield, 3.5km in basal diameter, the summit of which towers 470m above the caldera seafloor. The magmatic vents of both, lie within a NE-SW volcanotectonic line which controls the magma ascent of the region.

The evolution of the Kameni islands has been determined by 9 subaerial eruptions: 197 BCE, AD46-47, AD726, 1570-1573, 1707-1711, 1866-70, 1925-28, 1939-41, and 1950 (Pyle and Elliot, 2006) that discharged dacitic flows and formed domes, channels and levees, blocky lavas, ash plumes (Vulcanian eruptions) and ballistic ejecta. Bathymetric imagery data have revealed unknown submarine flows (pillow lavas) defining the actual morphology (pillow lavas) and final volume of products from Kameni Volcano to $4.85 \pm 0.7 \text{ km}^3$ (Nomikou et al., 2014).

The 1570-1573 AD volcanic crater is located in the northeastern part of it. During its surtseyan activity which was accompanied by ash-fall and block fall-out, a small lava dome named Mikri Kameni was extruded (Watts et al., 2015).
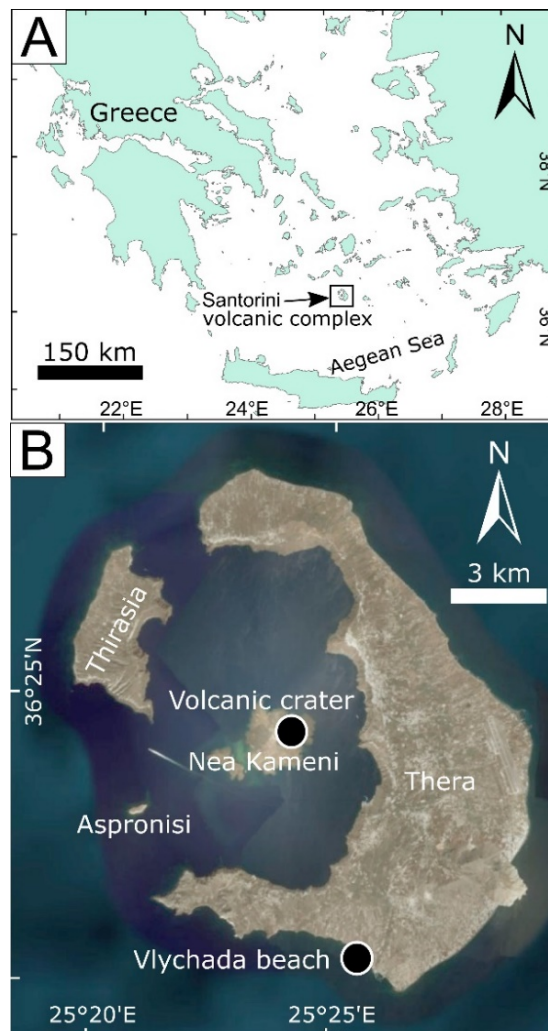
Figure 1: Location of Santorini group in the Aegean Sea (A) and selected sites belonging to Santorini Volcanic Complex (B).

Moving to the external southern part of Thera island, and along Vlychada beach, a very well exposed section with pumice layers deposited during the famous Late Bronze Age (LBA) (well-known also as Minoan) eruption, can be seen. The LBA eruption of Santorini has influenced the decline of the great Minoan civilization on Crete, making it an iconic event in both volcanology and archaeology (e.g., Manning et al. 2006; Druitt, 2014). It discharged between 30 and 80km^3 (dense rock equivalent; Johnston et. al., 2014) of rhyodacitic magma, mostly

as pyroclastic flows which entered the sea, and are preserved as ignimbrite in the surrounding submarine basins (Sigurdsson et. al., 2006). According to numerous volcanological studies, there is a consensus that the eruption occurred in four major phases with an initial precursory phase (Reck, 1936; Heiken and McCoy, 1990; Druitt, 2014). In Vlychada, volcanic products from phases P2 and mostly P3 and P4 can be recognized. Phase P2 products are dominated by pyroclastic surge deposits with multiple bedsets, dune-like bedforms with wavelengths of several meters or more, bomb sag horizons, and TRM temperatures of 100–250°C. Phase P3 is a coarse-grained, massive, phreatomagmatic ignimbrite up to 55m thick (Druitt et al., 1999), still reflecting magma-water interaction and deposited at low temperatures (Druitt, 2014; McClelland E. & Thomas R. A.,1990). Phase P4 is a tan- to pink- colored compound ignimbrite ("tan ignimbrite") (Druitt, 2014), mostly finegrained (ash and lapilli grade), with a high abundance of comminuted lithic debris in the ash fraction (Bond and Sparks, 1976) (Fig. 2B).
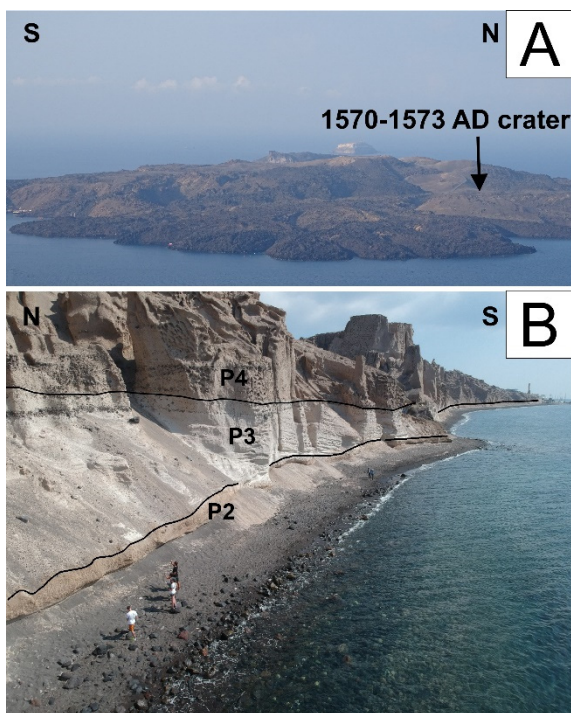

Figure 2: (A) Panoramic view of Nea Kameni island, the location of 1570-1573 crater is indicated. (B) UAV-captured picture showing part of the LBA deposit outcropping along the Vlychada beach, the recognizable phases (P2, P3 and P4) are indicated.

3   3D MODELLING

In this section we present the used workflow, aimed at 3D DOMs construction, which can be divided in three parts: *i)* appropriate UAV selection, *ii)* data collection (digital image gathering and setup of Ground Control Points - GCPs), and *iii)* SfM-MVS photogrammetry processing - data processing and model reconstruction. The results are in the form of Digital Surface Models (DSMs), Orthomosaics and 3D DOMs (or Virtual Outcrops).

3.1   UAV Selection and Use

For the present research, a commercial multi-rotor vehicle has been chosen, since it can be remotely controlled, is characterized by a stable hovering, can be easily transported in the field and is less expensive than hybrid and fixed-wing models. In addition, it can fly at very low heights, thus obtaining greater field resolution, while take-off and landing operations are smoother compare to that of fixed-wing models and this can be crucial especially when operating in difficult logistic terrains, such as lava flow outcrops or remote beach areas (Bonali et al., 2019a; Fallati et al., 2019). Having that in mind, we selected the DJI Spark "selfie drone" (Fig. 3), being a 0.300-kg vehicle equipped with a 1/2.3 inch CMOS sensor capable of capturing 12 Megapixel pictures, including EXIF information (Exchangeable Image file Format) GPS geographic coordinates (DATUM WGS84), and video up to 1080p at 30 fps, while its storage capacity is up to 64 GBs via a Micro SD card. Its flight time is approximately 16 minutes, thus four batteries and an external charger (since it can be also charged by USB plug) were used for the survey. The camera is attached to a 2-axis mechanical gimble that provides stabilization, allowing to capture clear, stable images and video, having a tilting range of 0-85°. Owing to its small size and low weight, we retain that this model is useful for field research and 3D DOM reconstruction, particularly for outcrops located in very remote areas where the equipment must be carried on foot.

3.2   Flight Mission and Data Collection

The first step has been devoted to defining the area to be surveyed and to planning the details of the flight missions, such as path orientation. In doing this, care must be taken of wind direction, which may affect UAV flight performance. As the surveyed geological objects are situated in very remote areas, we made use of the smaller DJI Spark, managed through the DJI

GO App (https://www.dji.com/it/goapp). Generally, mission planning involves fundamental parameters like path orientation, overlaps of images, flight height, flight speed, also depending on camera characteristics (e.g. Bonali et al., 2019). Such parameters influence the quality of the generated products (3D point cloud, DSM, orthomosaic, 3D Model). As suggested in recent works (Gerloni et al., 2018; Antoniou et al. 2019; Bonali et al. 2019a; Krokos et al. 2019), UAV-captured photos should have an overlap of 90% along single paths and 80% in a lateral direction, so as to obtain a better alignment of the images and reduce distortions on the resulting orthomosaics. The UAV we tested does not use any autopilot system, so that it has been manually controlled by the pilot for the entire duration of the mission. We are aware that not using mission planning software can affect the final quality of the model, but it was one of the challenge of the present work).

Figure 3: The selfie drone used in the present work, also equipped with propeller guards, person for scale.

In order to reach the goals of the present work, during image collection pictures were taken from a height lower than 30 m, the drone flew at a speed of 2 m/s with an overlap consistently in a range of 90-85% along paths and 80-75% in a lateral direction; images were captured every 2 seconds (equal time interval mode), and in optimal light conditions, suitable for the camera ISO range (100-1600). This was done to minimize the motion blur, to avoid the rolling shutter effect, and to achieve well-balanced camera settings (exposure time, ISO, aperture), thus ensuring sharp and correctly exposed images (e.g. Vollgger et al. 2016). Moreover, to reduce shadows around elevated features, drone was operated when

the sun was straight overhead (at zenith). In order to allow the co-registration of datasets and the calibration of models resulting from SfM-MVS photogrammetry processing (e.g. James and Robson, 2012; Turner et al., 2012; Westoby et al., 2012; James et al., 2017), World Geodetic System (WGS84) coordinates of, at least, four artificial Ground Control Points (GCPs) were fixed near every corner of each surveyed area (an additional one was selected in the central part) reducing the 'doming' effect resulting from SfM processing.

3.3 Photogrammetry Processing

After photo collection, the next step is dedicated to data processing aimed at 3D DOMs, DSMs and Orthomosaics generation. The collected images have been processed through Agisoft Metashape (http://www.agisoft.com/), a commercial Structure from Motion software (SfM). This application has been increasingly used for both UAV and field based SfM reconstructions, owing to its user-friendly interface, intuitive workflow and high quality of point clouds (Burns et al., 2017).
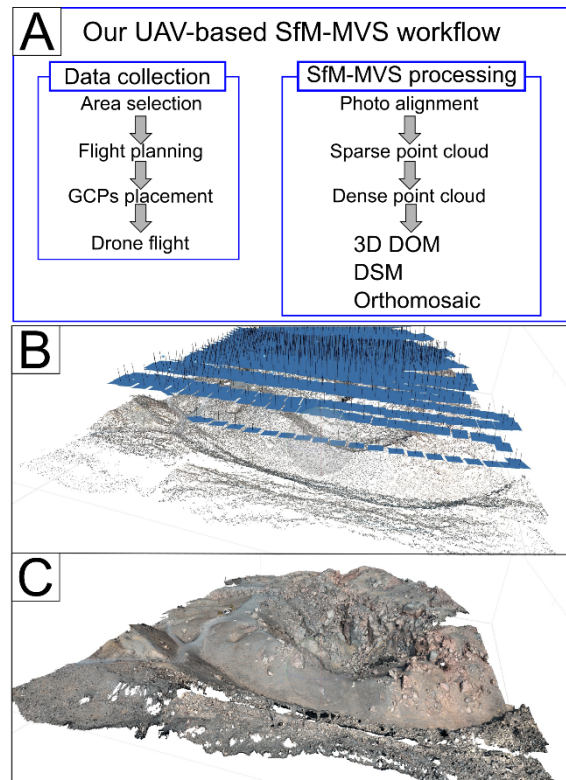

Figure 4: (a) UAV-based SfM-MVS Workflow used, (b) UAV-collected pictures already aligned with the processed sparse cloud. (c) Dense cloud generated by the SfM software showing the 1570-1573 Volcanic Crater.

SfM-MVS techniques allowed us to identify matching features in different photos and combine them to create a sparse and a dense cloud, an orthomosaic, a DSM, and eventually a 3D DOMs as final products (Stal et al., 2012; Westoby et al., 2012). The steps leading to model construction are shown in Figure 4A; further details are provided hereunder. The first step was to obtain an initial low-quality photo alignment, only considering measured camera locations. Thereafter, we excluded the photos with quality value <0.8 (or out of focus) from any further processing, using the tool provided by the software that is designed to detect poorly focused images (Agisoft L.L.C, 2020). Following this initial quality check, Ground Control Points (GCPs) were added to all photos, where available, so as to: *i)* scale and georeference the point cloud (and thus the resulting model); *ii)* optimize extrinsic parameters, such as estimated camera locations and orientations; *iii)* improve the accuracy of the final model. Photos were then realigned in high quality setting, camera locations and orientations were better established, and the sparse point cloud was computed by the software (e.g. Fig. 4B). The next phase consisted in reconstructing the dense point cloud (e.g. Fig. 4C) from the sparse point cloud, using a mild depth filtering and medium quality settings. The 3D DOMs, DSMs and orthomosaics were finally created through the Agisoft Metashape software. The resulting 3D DOMs are characterized by a high-resolution texture with a pixel size < 1.0 cm/pixel.

3.4 Georeferencing of GCPS

In order to allow the co-registration of datasets and calibration of models as well as for reducing the 'doming' effect resulting from SfM processing (e.g. Orthomosaics and DSMs), World Geodetic System (WGS84) coordinates of, at least, four artificial Ground Control Points (GCPs) were established near each corner and another one in the central part of each surveyed area (e.g. James and Robson, 2012; Turner et al., 2012; Westoby et al., 2012; James et al., 2017). For surveying GCPs, we placed well visible artificial markers, as well as natural targets (e.g. lava flow borders). GCPs were surveyed with the Emlid Reach RS©, low-cost single frequency receivers (Rover and Base) in RTK configuration (with centimetre-level accuracy). In regard to the surveys in Santorini, we used the Long-Range Radio (LoRa 868/915 MHz) connection mode where the base was set on a fix position and sent a real-time correction to the Rover. The LoRa mode can be advantageous in the absence of international GNSS service or CORS network. All

the z (altitude a.s.l.) values of the GCPs were corrected using the regional geoid model to obtain the orthometric height for the models.

4   RESULTS

In this section we provide all details regarding the 3D DOMs, DSMs and orthomosaic for the two studied areas, including new 2D and 3D maps, data and interpretations.

4.1   Volcanic Crater in Nea Kameni

A total number of 1522 of pictures have been collected using nadir camera orientation and 1231 of them have been correctly aligned and used for the dense cloud generation. The remnant 291 have been excluded because they resulted out of focus, too dark or too white, or below the quality threshold value of 0.8 applied for this model.

The resulting model for the 1570-1573 volcanic crater has an overall extent of 207x 291 m, a resolution of 3.79 cm/pix for the DSM and of 9.47 mm/pix for both the orthomosaic and the texture of the 3D DOM. The DSM values are in the range of 11.02- 49.15 m above the sea level (a.s.l.) (Fig. 4). By analysing the Orthomosaic, DSM and the 3D DOM we also recognised the following features: *i)* the crater is slightly elongated along N5°E direction (102.52 x 95.33 m); *ii)* by 3D analysis it is possible to trace the line connecting the two crater rim depressed points (e.g. Tibaldi, 1995; Bonali et al., 2011) in the same direction; *iii)* in the northernmost part of the crater an open fracture with a dilation of 4.7-5.3 m is present and *iv)* the crater has a depth of 31.43 m.

4.2   Volcanic Deposit along the Vlychada Beach

A total number of 568 pictures have been collected and considering the geometry of the outcrops, that is almost vertical, the majority of them have been collected with an oblique camera orientation.

439 of them have been correctly aligned and used for the dense cloud generation, whereas 129 have been excluded, using the same method as in the previous mentioned model. In addition, a mask has been applied to all photos, in order to exclude the sky and the sea water from the processing, to avoid artefacts and noises. The model for the volcanic deposit surveyed along the Vlychada beach has an overall extent of 157 x 128 m, a resolution of 1.67

cm/pix for the DSM and of 8.37 cm/pix for both the orthomosaic and the texture of the 3D DOM.

The DSM values are in the range -1.61- 38.3m a.s.l.. Regarding the volcanic phases that can be recognised, it resulted very useful to collect the thickness of them directly on the 3D DOM, because of the vertical geometry of the outcrop. These measurements have been collected in Agisoft Metashape, using the ruler tool: the phase 2 has a thickness of 2m, phase 3 ranges between 7 and 10 m and phase 4 has an outcropping thickness of 25m. In addition, it is possible to appreciate the presence of several blocks as well as to quantify their dimension as shown in Figure 5D.

5 DISCUSSION

In the present section we discuss the use of selfie drones for 3D modelling and mapping, as well as we present new outcomes for the studied areas.

5.1 Selfie Drones for Surveying, 3D Modelling and Mapping

At a general level, UAVs are excellent instruments to collect highly detailed pictures and videos from the above of the key sites (e.g. Fig. 2A), which is impossible using only classical field activity. These images can be used for research activity and better interpretation as well as for outreach activity (e.g. Bonali et al., 2019a; Pasquaré Mariotto et al., 2020). Furthermore, a field view from the drone during field surveys can also help in planning further steps of exploration. In view of the above, a selfie drone, due to its small dimension and weight, is useful in supporting field exploration and photo/video collection, even though it is recommended to work in the height and distance range suggested by local laws and manufacture's technical manual.

Regarding the 3D modelling, and consequent mapping and data collection activity, both models have great resolution, in terms of DSM and Orthomosaic. In particular, the latter and the texture of the 3D DOM, reach a resolution greater than 1 cm. This excellent resolution is helpful for classical mapping and data collection on DSM/Orthomosaic, as well as is crucial for mapping 3D vertical outcrops, including the quantitative characterisation of small objects like the ones included in the volcanic layers outcropping along the Vlychada beach. Based on the experience gained from the present work we were capable of flying up to 50 m from the ground to collect some pictures for the latter model.
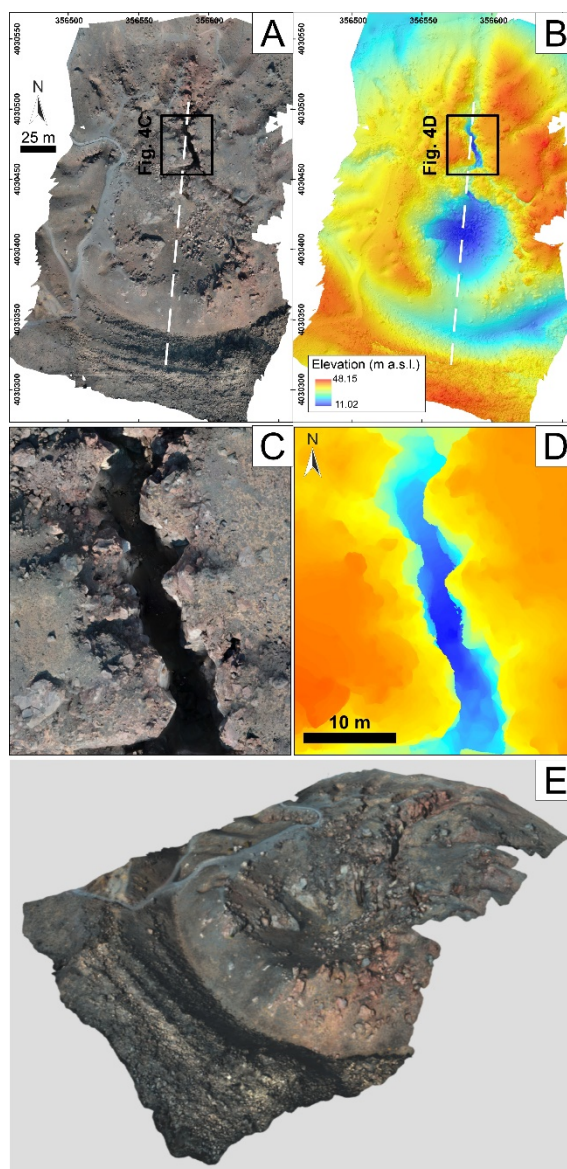

Figure 5: (A) Orthomosaic and DSM (B) of the 1570-1573 volcanic crater in Nea Kameni; a.s.l.: above the sea level. (C-D) Detailed view of the northernmost fracture. (E) 3D Virtual Outcrop of the volcanic crater available online (https://skfb.ly/6PUNt).

Respect to other models, there are some negative aspects that we highlighted. Selfie drones must be manually controlled during the survey and they can be more affected by the wind; so, an expert pilot is recommended to collect pictures in the best way possible. This can result in a larger number of collected pictures compared to those really needed for SfM-MVS processing, since some of them must be removed due to out of focus condition or incorrect white balance. To fly above 50 m and to cover larger

areas, other types of UAVs can be used: balloons, larger multi-rotor, fixed-wing and hybrid. Balloons do not need fuel or a battery, but they cannot be remotely controlled. The fixed-wing type can cover larger areas in a smaller time frame using high quality cameras, but such model is more difficult to be transported in the field. Hybrid types allow to switch between flying like a fixed-wing aircraft and hovering like a multi-rotor one. The latter two are more expensive than commercial multi-rotor type. Larger multi-rotor can fly for a longer time respect to a selfie drone, at very low heights attaining a great field resolution, and much more importantly, take-off and landing operations are easier than for fixed-wing models; this is crucial especially in difficult logistic terrains.
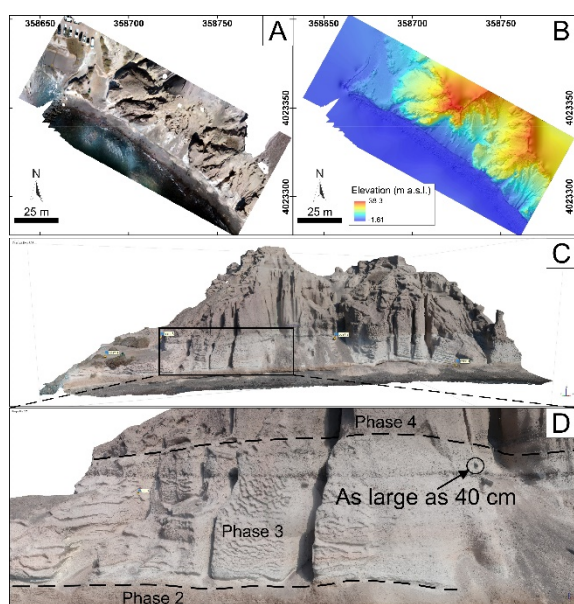

Figure 6: (A) Orthomosaic and DSM (B) of the outcrop related to LBA deposits along the Vlychada beach; a.s.l.: above the sea level. (C) 3D Virtual Outcrop available online (https://skfb.ly/6PZPO), where it is possible to recognise the different phases with very high detail (D).

5.2 New Outcomes for the Studied Areas

Regarding the 1570-1573 volcanic crater in Nea Kameni, we defined its dimension and depth with very high accuracy, also discovering a N5°E elongation trend that matches with the line connecting the two most depressed points along the crater rim. As suggested by Tibaldi (1995) and Bonali et al. (2011), such line can represent, with low discrepancy, the direction of magma feeding fractures, suggesting that the 1570-1573 AD eruptions were driven by a

fissure. Dykes outcropping along the Northern Caldera Wall have a NE-SW dominant strike, even though the N-S direction is also represented in the dataset (Browning et al., 2015), suggesting that magma can reach the surface also along this direction in central Santorini. Finally, the fracture located just north of the crater has a dilation of about 5 m that is consistent with dyke-induced fractures in Northern Iceland (e.g. Bonali et al., 2019a,b).

Regarding the volcanic deposits measured along the Vlychada beach, we defined the boundaries of different phases of the LBA deposits on the 3D DOM, as well as we measured their thickness with very high accuracy. Also, it was possible to observe the cliff closely enough to distinguish individual and small components such as volcanic blocks within the bulk of each phase and to quantify their dimensions.

5.3 3D DOMs and Virtual Outcrops for Teaching and Dissemination

The two presented sites can be used also for teaching and outreach activity, as well as they can be both suggested as geosites. In fact, they have a considerable scientific value and a potentially high educational value, enhanced by their accessibility and safety (e.g. Pasquaré Mariotto et al., 2020).

Recent improvements in Geographic Information Systems (GIS) technologies can provide new opportunities for immersive and wide engaging public audiences. Story Maps being interactive webGIS applications can provide support for scientific storytelling in a compelling and straightforward way (Antoniou, et al., 2019) using multi-media assets (e.g. photos, videos, 3D DOMs) and narrative texts with the aim of visualizing spatial data effectively.

As previously tested (Antoniou et al., 2018; 2019, 2019a, 2019b) these applications can represent an interactive way for presenting the geological and geomorphological characteristics of places which can be defined as geotopes or protected areas worldwide, providing a quick access of all useful data to a wide audience and thus developing the interest and possibly motivating people to learn more and visit the area.

With the purpose of enhancing the popularization and fruition of these two sites, we published them as "Virtual Outcrops" (Xu et al. 1999; Trinks et al. 2005; Tavani et al. 2014) on the web. The 1570-1573 AD volcanic crater is available as Virtual Outcrop at https://skfb.ly/6PUNt and the volcanic deposits section in Vlychada beach, at https://skfb.ly/6PZPO. Both of them can be visualized using a laptop or

mobile phone (in 2D) or using a Mobile VR headset to appreciate the third dimension (e.g. Fig. 6A).

Finally, as suggested by Gerloni et al. (2018) and Krokos et al. (2019), SfM-MVS-derived 3D DOMs can be imported in a game engine to build fully navigable immersive Virtual Reality systems. Such approach has been firstly used for teaching activity (e.g. Fig 6B) and dissemination activity to popularise geosciences to non-academic audiences (e.g. citizens).

Figure 7: (A) An example of a research group observing the same virtual outcrop using a mobile VR headset. (B) An example of an outreach event carried out using the Immersive Virtual Reality (Bonali et al., 2019c).

5.4 Future Developments

Regarding the future roadmap for our approach, we expect a contribution from Neanias project (https://www.neanias.eu/) regarding online services devoted to SfM-MVS photogrammetry processing, in order to enlarge the community working with this technique, possibly involving also non-scientists and non-academics. Up to now, we cannot find a robust and efficient open source software for SfM-MVS processing, that can be applied to both terrestrial and marine environments; for the latter case, pictures are usually collected using (Remotely Operated Vehicle) ROVs. From another side, the Selfie drone-based approach can motivate scientists to collect data in remote and dangerous areas, thus multiplying the amount of available 3D DOMs for the scientific community as well as the storage dimension needed for the DSMs, Orthomosaics and the dense clouds. In

view of the above, an online service for data storage and 3D scientific visualisation is also recommended. For example, the model related to the entire project of the 1570-1573 AD crater is as large as 54 GBs, and it is difficult to be shared with the scientific community, even though the high resolution of the 3D DOM, DSM and Orthomosaic can be crucial for better understanding volcano dynamics, relationships with release of volcanic gases, tectonic settings, magmatic intrusions.

6 FINAL REMARKS

In the present work we tested the use of selfie drones as a tool for 3D modelling, geological mapping and data collection. Test sites are located in Santorini and are characterised by different settings: i) the Crater area in Nea Kameni has a mostly horizontal topography; ii) the Vlychada beach has a dominant vertical topography. By applying the Structure from Motion techniques to pictures collected using the selfie drone, we were capable of: *i)* reconstructing the two sites with centimetric to sub-centimetric resolution; *ii)* recognizing geological features on very high resolution DSMs and Ortomosaics; *iii)* mapping vertical volcanic deposits on 3D DOMs; and *iv)* collecting new quantitative data for both sites.

REFERENCES

Agisoft, L. L. C. "Agisoft metashape user manual, Professional edition, Version 1.6." Agisoft LLC, St. Petersburg, Russia, from https://www.agisoft.com/pdf/metashape-pro_1_6_en.pdf, accessed March 12 (2020):2020.

Antoniou, V., Nomikou, P., Bardouli, P., Lampridou, D., Ioannou, Th., Kalisperakis, I., Stentoumis, Ch., Whitworth, M., Krokos, M. & Ragia, L. (2018). An Interactive Story Map for the Methana Volcanic Peninsula. In *Proceedings of the 4th International Conference on Geographical Information Systems Theory, Applications and Management* (GISTAM 2018), pages 68-78, ISBN: 978-989-758-294-3.

Antoniou, V.; Ragia, L.; Nomikou, P.; Bardouli, P.; Lampridou, D.; Ioannou, T.; Kalisperakis, I.; Stentoumis, C., 2018. Creating a Story Map Using Geographic Information Systems to Explore Geomorphology and History of Methana Peninsula. *ISPRS Int. J. Geo-Inf. 2018*, 7, 484.

Antoniou, V., Nomikou, P., Bardouli, P., Sorotou, P., Bonali, F.L., Ragia, L. and Metaxas, A., 2019. The Story Map for Metaxa Mine (Santorini, Greece): A Unique Site Where History and Volcanology Meet Each Other. In *Proceedings of the 5th International Conference on Geographical Information Systems Theory, Applications and Management* - Volume 1: GISTAM, 212-219.

Antoniou, V., Nomikou, P., Zafeirakopoulou, E., Bardouli, P., Ioannou, T., 2019a. Geo-biodiversity and cultural environment of Nisyros volcano. *15th International Congress of the Geological Society of Greece*, Sp. Pub. 7 Ext. Abs. GSG2019-195, Athens, 22-24 May, 2019, p. 716-717.

Antoniou, V., Nomikou, P., Papaspyropoulos, K., Vlasopoulos, O., Zafeirakopoulou, E., Bardouli, P., Chrysopoulou, E., 2019b. Geo-biodiversity and Cultural Environment of the regions surrounding the Corinth Gulf (Greece). *Regional Conference on Geomorphology, Focal Theme: Geomorphology of Climatically and Tectonically Sensitive Areas*, UNESCO Global Geoparks: geoheritage assessment and management - geo-tourism development, Abstract book, p.256, Athens 2019.

Bonali, F. L., Corazzato, C., Tibaldi, A., 2011. Identifying rift zones on volcanoes: an example from La Réunion island, Indian Ocean. *Bulletin of volcanology*, 73(3), 347-366.

Bonali, F. L., Corazzato, C., Tibaldi, A., 2012. Elastic stress interaction between faulting and volcanism in the Olacapato–San Antonio de Los Cobres area (Puna plateau, Argentina*). Global and planetary change*, 90, 104-120.

Bonali, F. L., Tibaldi, A., Marchese, F., Fallati, L., Russo, E., Corselli, C., Savini, A., 2019a. UAV-based surveying in volcano-tectonics: An example from the Iceland rift. *Journal of Structural Geology*, 121, 46-64.

Bonali, F. L., Tibaldi, A., Mariotto, F. P., Saviano, D., Meloni, A., Sajovitz, P., 2019. Geometry, oblique kinematics and extensional strain variation along a diverging plate boundary: The example of the northern Theistareykir Fissure Swarm, NE Iceland. *Tectonophysics*, 756, 57-72.

Bonali, F. L., Russo, E., Savini, A., Marchese, F., Fallati, L., Paraskevi, N., ... Garzonio, R., 2019c. Learning outcomes from the EGU 2018 Public Engagement grant" Shaping geological 3D virtual field-surveys for overcoming motor disabilities". In *Geophysical Research Abstracts*, Vol. 21.

Bond, A. & Sparks, R.S.J., 1976. The Minoan eruption of Santorini, Greece, *Journal of the Geological Society*, London, 132, 1–16.

Browning, J., Drymoni, K., Gudmundsson, A., 2015. Forecasting magma-chamber rupture at Santorini volcano, Greece. *Scientific reports*, 5, 15785.

Burns, J.H.R., Delparte, D., 2017. Comparison of commercial structure-from-motion photogrammetry software used for underwater three-dimensional modeling of coral reef environments. In *International Archives of the Photogrammetry, Remote Sensing and Spatial Information Sciences* - ISPRS Archives (Vol. 42, pp. 127–131).

Druitt, T. H. & Francaviglia, V., 1992. Caldera formation on Santorini and the physiography of the islands in the late Bronze Age, *Bull. Volcanol.*, 54, 484–493.

Druitt, T. H., 2014. New insights into the initiation and venting of the Bronze-Age eruption of Santorini (Greece), from component analysis, *Bull. Volcanol.*, 76, 794.

Fallati, L., Polidori, A., Salvatore, C., Saponari, L., Savini, A., Galli, P., 2019. Anthropogenic Marine Debris assessment with Unmanned Aerial Vehicle imagery and deep learning: A case study along the beaches of the Republic of Maldives. *Science of The Total Environment*, 693, 133581.

Friedrich, W., Kromer, B., Friedrich, M., Heinemeier, J., Pfeiffer, T., Talamo, S., 2006. Santorini eruption radiocarbon dated to 1627–1600 Bc., *Science*, 312, 548.

Gerloni, I.G., Carchiolo, V., Vitello, F.R., Sciacca, E., Becciani, U., Costa, A., Riggi S., Bonali F.L., Russo E., Fallati L., Marchese F., Tibaldi A., 2018. Immersive Virtual Reality for Earth Sciences. In *2018 Federated Conference on Computer Science and Information Systems* (FedCSIS) (pp. 527-534). IEEE.

James, M.R., Robson, S., 2012. Straightforward reconstruction of 3D surfaces and topography with a camera: accuracy and geoscience application. *Journal of Geophysical Research*, 117, F03017.

James, M.R., Robson, S., d'Oleire-Oltmanns, S., Niethammer, U., 2017. Optimising UAV topographic surveys processed with structure-from-motion: ground control quality, quantity and bundle adjustment. *Geomorphology*, 280, 51-66.

Johnston, E. N., Sparks, R.S.J., Phillips, J.C. & Carey, S., 2014. Revised estimates for the volume of the Late Bronze Age Minoan eruption, Santorini. Greece, *J. Geol. Soc. Lond.*, 171, 583–590.

Krokos M., Bonali F., Vitello F., Antoniou V., Becciani U., Russo E., Marchese F., Fallati L., Nomikou P., Kearl M., Sciacca, E., Whitworth M., 2019. Workflows for virtual reality visualisation and navigation scenarios in earth sciences. In *5th International Conference on Geographical Information Systems Theory, Applications and Management*: GISTAM 2019. SciTePress.

Manning, S.W., Ramsey, C.B., Kutschera, W., Higham, T., Kromer, B., Steier, P., Wild, E.M.,2006. Chronology for the Aegean Late Bronze Age 1700–1400 B.C., *Science*, 312, 565–569.

Nomikou P., Papanikolaou D., Alexandri M., Sakellariou D., Rousakis G., 2013. Submarine volcanoes along the Aegean volcanic arc. *Tectonophysics*, 597-598, pp.123.

Nomikou, P., Parks M.M., Papanikolaou D., Pyle D.M., Mather T.A., Carey S., Watts A.B., Paulatto M., Kalnins M., Livanos I., Bejelou K., Simou E., Perros I., 2014. The emergence and growth of a submarine volcano: The Kameni islands, Santorini (Greece). *GeoResJ*, 1-2, pp.8.

Pasquaré Mariotto, F., Bonali, F.L., Venturini, C., 2020. Iceland, an open-air museum for geoheritage and Earth Science communication purposes. *Special Issue "Geoheritage and Geotourism Resources"*, accepted for publication.

Pyle, D.M., Elliott, J.R., 2006. Quantitative morphology, recent evolution, and future activity of the Kameni Islands volcano, Santorini, Greece. *Geosphere*, 2(5), 253-268.

Reck, H., 1936. *Santorini: Der Werdegang eines Inselvulkans und sein Ausbruch*, 1925–1928, Reinser, Berlin.

Sigurdsson, H., Carey, S., Alexandri, M., Vougioukalakis, G., Croff, K., Roman, C., Sakellariou, D., Anagnostou, C., Rousakis, G., Ioakim, C., Gogou, A., Ballas, D., Misaridis, T., Nomikou, P., (2006). Marine Investigations of Greece's Santorini Volcanic Field. *Eos 87* (34), pp.337.

Stal, C., Bourgeois, J., De Maeyer, P., De Mulder, G., De Wulf, A., Goossens, R., Hendrickx, M., Nuttens, T., Stichelbaut, B., 2012. Test case on the quality analysis of structure from motion in airborne applications. In *32nd EARSeL Symposium: Advances in geosciences*. European Association of Remote Sensing Laboratories (EARSeL).

Tavani, S., Granado, P., Corradetti, A., Girundo, M., Iannace, A., Arbués, P., Muñozb J.A., Mazzoli, S., 2014. Building a virtual outcrop, extracting geological information from it, and sharing the results in Google Earth via OpenPlot and Photoscan: An example from the Khaviz Anticline (Iran). *Computers & Geosciences*, 63, 44-53.

Tibaldi, A., 1995. Morphology of pyroclastic cones and tectonics. *Journal of Geophysical Research: Solid Earth*, 100 (B12), 24521-24535.

Tibaldi, A., Pasquarè, F. A., Papanikolaou, D., Nomikou, P., 2008. Discovery of a huge sector collapse at the Nisyros volcano, Greece, by on-land and offshore geological-structural data. *Journal of volcanology and geothermal research*, 177 (2), 485-499.

Tibaldi, A., Alania, V., Bonali, F. L., Enukidze, O., Tsereteli, N., Kvavadze, N., Varazanashvili, O., 2017. Active inversion tectonics, simple shear folding and back-thrusting at Rioni Basin, Georgia. *Journal of Structural Geology*, 96, 35-53.

Trinks, I., Clegg, P., McCaffrey, K., Jones, R., Hobbs, R., Holdsworth, B., Holliman N., Imber, J., Waggott, S., Wilson, R., 2005. Mapping and analysing virtual outcrops. *Visual Geosciences*, 10(1), 13-19.

Turner, D., Lucieer, A., Watson, C., 2012. An automated technique for generating georectified mosaics from ultra-high resolution unmanned aerial vehicle (UAV) imagery, based on structure from motion (SfM) Point clouds. *Remote sensing*, 4, 1392-1410.

Vollgger, S.A. and Cruden, A.R., 2016. Mapping folds and fractures in basement and cover rocks using UAV photogrammetry, Cape Liptrap and Cape Paterson, Victoria, Australia. *Journal of Structural Geology*, 85, 168-187.

Watts, A.B., Nomikou P., Moore J.D.P., Parks M.M., Alexandri M., 2015. Historical bathymetric charts and the evolution of Santorini submarine volcano, Greece. *Geochemistry, Geophysics, Geosystems*, 16 (3), pp.847.

Westoby, M.J., Brasington, J., Glasser, N.F., Hambrey, M.J., Reynolds, J.M., 2012. "Structure-from-Motion" photogrammetry: a low-cost, effective tool for geoscience applications. *Geomorphology*, 179, 300-314.

Westoby, M.J., Brasington, J., Glasser, N.F., Hambrey, M.J., Reynolds, J.M., 2012. "Structure-from-Motion" photogrammetry: a low-cost, effective tool for geoscience applications. *Geomorphology*, 179, 300-314.

Xu, X., Aiken, C.L., Nielsen, K.C., 1999. Real time and the virtual outcrop improve geological field mapping. *Eos, Transactions American Geophysical Union*, 80(29), 317-324.